# Island Cells Control Temporal Association Memory

Takashi Kitamura *et al.*

*Science* **343**, 896 (2014);
DOI: 10.1126/science.1244634

31. M. E. Hasselmo, J. McGaughy, *Prog. Brain Res.* **145**, 207–231 (2004).
32. L. F. Agnati *et al*., *Acta Physiol. (Oxf.)* **187**, 329–344 (2006).
33. L. M. Teles-Grilo Ruivo, J. R. Mellor, *Front. Synaptic Neurosci.* **5**, 2 (2013).
34. T. Klausberger *et al*., *Nature* **421**, 844–848 (2003).
35. D. L. F. Garden, P. D. Dodson, C. O'Donnell, M. D. White, M. F. Nolan, *Neuron* **60**, 875–889 (2008).
36. L. M. Giocomo, M. E. Hasselmo, *J. Neurosci.* **28**, 9414–9425 (2008).
37. F. R. Fernandez, J. A. White, *J. Neurosci.* **28**, 3790–3803 (2008).
38. L. M. Giocomo *et al*., *Cell* **147**, 1159–1170 (2011).
39. S. J. Zhang *et al*., *Science* **340**, 1232627 (2013).
40. D. C. Rowland, M.-B. Moser, *Curr. Opin. Neurobiol.* **24**, 22–27 (2014).
41. M. Brecht *et al*., *Philos. Trans. R. Soc. London B Biol. Sci.* **369**, 20120521 (2013).
42. T. A. Woolsey, H. Van der Loos, *Brain Res.* **17**, 205–242 (1970).
43. K. C. Catania, R. G. Northcutt, J. H. Kaas, P. D. Beck, *Nature* **364**, 493 (1993).

**Acknowledgments:** This work was supported by Humboldt Universität zu Berlin, Bernstein Center for Computational Neuroscience Berlin [German Federal Ministry of Education and Research (BMBF), Förderkennzeichen 01GQ1001A], NeuroCure, the Neuro-Behavior European Research Council grant, and the Gottfried Wilhelm Leibniz Prize of the Deutsche Forschungsgemeinschaft. We thank C. Ebbesen, M. von Heimendahl, R. Rao, J. Steger, J. Tukker, U. Schneeweiß, P. Turko, and I. Vida.

**Supplementary Materials**
www.sciencemag.org/content/343/6173/891/suppl/DC1
Materials and Methods
Figs. S1 to S6
References (*44*–*57*)

10 July 2013; accepted 19 December 2013
Published online 23 January 2014;
10.1126/science.1243028

# Island Cells Control Temporal Association Memory

**Takashi Kitamura,[1]* Michele Pignatelli,[1]* Junghyup Suh,[1] Keigo Kohara,[1] Atsushi Yoshiki,[2] Kuniya Abe,[2] Susumu Tonegawa[1,3]†**

**Episodic memory requires associations of temporally discontiguous events. In the entorhinal-hippocampal network, temporal associations are driven by a direct pathway from layer III of the medial entorhinal cortex (MECIII) to the hippocampal CA1 region. However, the identification of neural circuits that regulate this association has remained unknown. In layer II of entorhinal cortex (ECII), we report clusters of excitatory neurons called island cells, which appear in a curvilinear matrix of bulblike structures, directly project to CA1, and activate interneurons that target the distal dendrites of CA1 pyramidal neurons. Island cells suppress the excitatory MECIII input through the feed-forward inhibition to control the strength and duration of temporal association in trace fear memory. Together, the two EC inputs compose a control circuit for temporal association memory.**

Episodic memory consists of associations of objects, space, and time (*1*). In humans and animals, the entorhinal cortex (EC)–hippocampal (HPC) network plays an essential role in episodic memory (*2*), with medial EC (MEC) and lateral EC (LEC) inputs into HPC providing spatial and object information, respectively (*3*). Neural circuits have been identified in the EC-HPC network that mediate space and object associations (*4*–*6*). In contrast, the neural circuits for time-related aspects of episodic memory are only beginning to be studied (*7*, *8*). Direct inputs from MEC layer III (MECIII) cells to CA1 pyramidal cells drive the temporal association of discontiguous events (*9*). Like most cognitive and motor phenomena, temporal association memory must be regulated for optimal adaptive benefit, yet nearly nothing is known about the underlying mechanisms of this regulation. We investigated this issue by mapping and characterizing an unsuspected neuronal circuit within the EC-HPC network and examining the effect of its optogenetic manipulations on a temporal association memory.

A retrograde tracer, cholera toxin subunit B (CTB), was injected into the dentate gyrus (DG) of C57BL6 mice (Fig. 1A). Although a majority of cells in EC layer II (ECII) were CTB-positive, a large proportion was CTB-negative and clustered in a series of about 130-μm-diameter bulblike structures (Fig. 1, B and C). Hereafter, we refer to these CTB-negative cells as ECII island (ECIIi) cells. ECIIi cells are mostly pyramidal (Fig. 1F and fig. S1) and express Wfs1 (*10*) and calbindinD-28K (*11*) (Fig. 1, B to D and F). CTB-positive cells were identified as previously well known DG-projecting stellate cells (*12*, *13*) (Fig. 1G and figs. S1 and S2) that express reelin (*14*) but not Wfs1 or calbindinD-28K (Fig. 1E). Hereafter, we refer to these CTB-positive cells as ECII ocean (ECIIo) cells. ECIIi cells are excitatory (Fig. 1F and figs. S1 and S2) and present in both MEC and LEC (fig. S2), but they are distinct from ECIIo cells not only by their morphology and molecular markers but also by their intrinsic electrophysiological properties (*15*, *16*) (fig. S1).

We created a Cre transgenic mouse line by using the Wfs1 promoter (fig. S3). When the Cre-dependent adeno-associated virus encoding double-floxed inverted open reading frame with enhanced yellow fluorescent protein under control of elongation factor 1 α promoter (AAV9-EF1α-DIO-eYFP) was injected into the superficial layers of the EC (Fig. 1H), eYFP expression was restricted to Wfs1- and calbindinD-28K–positive ECIIi cells (Fig. 1, I and J, and fig. S4). These ECIIi cells appeared in a curvilinear matrix of bulblike structures in tangential MEC sections (Fig. 1K). We injected the $AAV_9$-EF1α-DIO-ChR2-eYFP virus (where ChR2 indicates channelrhodopsin-2) (*17*) into the EC of Wfs1-Cre mice (Fig. 1L). ECIIi cells projected primarily to the CA1 region via the temporoammonic pathway (Fig. 1M). Additional weaker projections were detected in the subiculum, parasubiculum, and contralateral CA1 and EC (Fig. 1M and fig. S5). Wfs1- and calbindinD-28K–positive ECIIi cells are also present in rat and project to the CA1 region (fig. S6).

In the CA1 region, ECIIi axons specifically innervated the border between the stratum radiatum (SR) and stratum lacunosum-moleculare (SLM) (Fig. 2A), terminating sharply at the proximal end of CA1, and did not enter into CA2 (Fig. 2A), which was marked with regulator of G protein signaling 14 (RGS14) (*18*). ECIIi axons were strongly myelinated (fig. S7) (*19*) and preferentially innervate the stratum lacunosum (SL) (Fig. 2B). In contrast, MECIII axons innervate the stratum moleculare (SM) immediately adjacent to the SL (Fig. 2C). Experiments conducted with a ChR2eYFP transgenic mouse line under control of vesicular γ-aminobutyric acid (GABA) transporter promoter (VGAT-ChR2eYFP) (*20*) and immunohistochemistry of glutamate decarboxylase 67 (GAD67) suggested that the primary target of the ECIIi cells are GABA-releasing interneurons in the SL (SL-INs) (Fig. 2, D to F) (*21*). Presynaptic terminal analysis showed ECIIi cells are glutamatergic (Fig. 2G and fig. S8). Low expression of PSD-95 in the SL suggested that innervations of ECIIi axons onto CA1 pyramidal cell dendrites in the SL are relatively infrequent (fig. S9).

Optogenetic stimulation of ChR2-expressing ECIIi axons during in vitro patch-clamp recordings of SL-INs revealed reliable excitatory postsynaptic currents (EPSCs, average amplitude of 54 ± 7 pA, average onset of 2.05 ± 0.07 ms, $n = 40$) in 87% of SL-INs ($n = 53$; Fig. 2, H to J, and fig. S10), which were sensitive to ionotropic glutamate receptor antagonists (fig. S11). In current mode, repetitive photostimulation was sufficient to trigger action potentials in SL-INs ($n = 14$ out of 40; Fig. 2, K and Q). Under similar stimulation conditions, CA1 pyramidal cells showed small EPSCs (average amplitude of 19 ± 5 pA, average onset of 3.11 ± 0.08 ms, $n = 29$) in 70% of them ($n = 50$; Fig. 2, L to N, and fig. S11), suggesting a weaker impact of ECIIi cells to CA1 pyramidal cells than to SL-INs

[1]RIKEN-MIT Center for Neural Circuit Genetics at the Picower Institute for Learning and Memory, Department of Biology and Department of Brain and Cognitive Sciences, Massachusetts Institute of Technology (MIT), Cambridge, MA 02139, USA. [2]RIKEN BioResource Center, 3-1-1 Koyadai, Ibaraki 305-0074, Japan. [3]Howard Hughes Medical Institute at MIT, Cambridge, MA 02139, USA.

*These authors contributed equally to this work.
†Corresponding author. E-mail: tonegawa@mit.edu

(Fig. 2P). In current mode, repetitive photostimulation never triggered action potentials in CA1 pyramidal cells ($n$ = 35). However, somatic depolarization to –55 mV revealed strong inhibitory potentials (IPSPs) in 30% of CA1 pyramidal cells ($n$ = 50, Fig. 2O) in response to optogenetic stimulation of ECIIi axons, which was abolished by bath application of GABA receptor antagonists (Fig. 2R). These data demonstrate a previously unknown feedforward inhibitory circuit controlled by ECIIi cells (Fig. 2S).

Input selectivity to SL-INs was investigated by replacing the Wfs1-Cre transgenic mice with the MECIII cell–specific pOxr1-Cre mice (*9*) or the CA3 cell–specific KA1-Cre transgenic mice (*5*) (Fig. 3, A to C). SL-INs were preferentially innervated by ECIIi cells (Fig. 3, D to G, and supplementary statistics).

The SL-INs exert an inhibitory effect on the apical dendrite of CA1 pyramidal cells (*22*). To investigate whether the ECIIi-SL-INs circuit has the ability to inhibit MECIII inputs to CA1 pyramidal cells, we injected the $AAV_9$-EF1α-DIO-ChR2-eYFP virus into the EC of pOxr1-Cre mice. We then simultaneously recorded connected pairs of SL-INs and CA1 pyramidal cells (Fig. 3H) to test whether SL-INs activity was sufficient to inhibit MECIII input. We found 8 connected pairs out of 260 tested pairs ($P_{connection}$ = 0.03, average unitary EPSP (uEPSP) amplitude of –0.18 ± 0.09 mV, average uIPSP onset of 1.45 ± 0.2 ms, Fig. 3I). A confocal microscopic analysis suggested an average of 2 ± 0.3 putative synaptic contacts between SL-INs axons and CA1 pyramidal cell's apical dendrites (Fig. 3H inset and fig. S12). By eliciting a brief burst in SL-INs, we observed IPSPs in all the connected CA1 pyramidal cells (Fig. 3J). Optogenetic stimulation of MECIII axons elicited EPSPs in CA1 pyramidal cells (Fig. 3K). However, pairing optogenetic and SL-IN stimulations significantly reduced the amplitude of EPSP to 60% of the response evoked by MECIII axonal stimulation alone (average amplitude of MEC stimulation only was 1.6 ± 0.4 mV; for pairing MEC and SL-INs, 0.9 ± 0.4 mV; $n$ = 8, Fig. 3, K and L). The lack of significant difference between the average IPSP amplitude and the inhibited component of the response suggested a reduction mediated mainly by linear subtraction (Wilcoxon signed-rank $P$ = 0.5).

We then sought the functional importance of ECIIi–SL-IN circuit-mediated inhibition of MECIII input to CA1 at the behavioral level. For this purpose, we injected bilaterally $AAV_9$-CBA-DIO-ArchT-eGFP (*23*) into the EC of pOxr1-Cre mice. Unilateral shining of green light to a CA1 area of these mice with an optic fiber implanted to this area (*24*) (Fig. 4A and fig. S13) inhibited the ArchT-expressing MECIII axons resulting in a reduction of the multiunit activity of CA1 pyramidal cells in vivo (58% reduction, Fig. 4B). We subjected mice to trace fear conditioning (TFC) while delivering green light bilaterally to the CA1 areas during the entire training period (i.e., three rounds of tone, trace, and shock periods). Mice expressing ArchT, but not control mice expressing the fluorescence marker only (i.e., tdTomato), exhibited severe freezing deficits during both training and testing sessions (Fig. 4, C and D) but not in response to the context (fig. S15). The remaining freezing observed during the tone period of the testing session is likely due to nonassociative learning (fig. S14).

We injected bilaterally $AAV_9$-EF1α-DIO-ChR2-eYFP into the EC of Wfs1-Cre mice. Unilateral shining of blue light to a CA1 area resulted in reduced multiunit activity of CA1 pyramidal cells in vivo (46% reduction, Fig. 4B), strongly supporting the feed-forward inhibition of CA1 activity

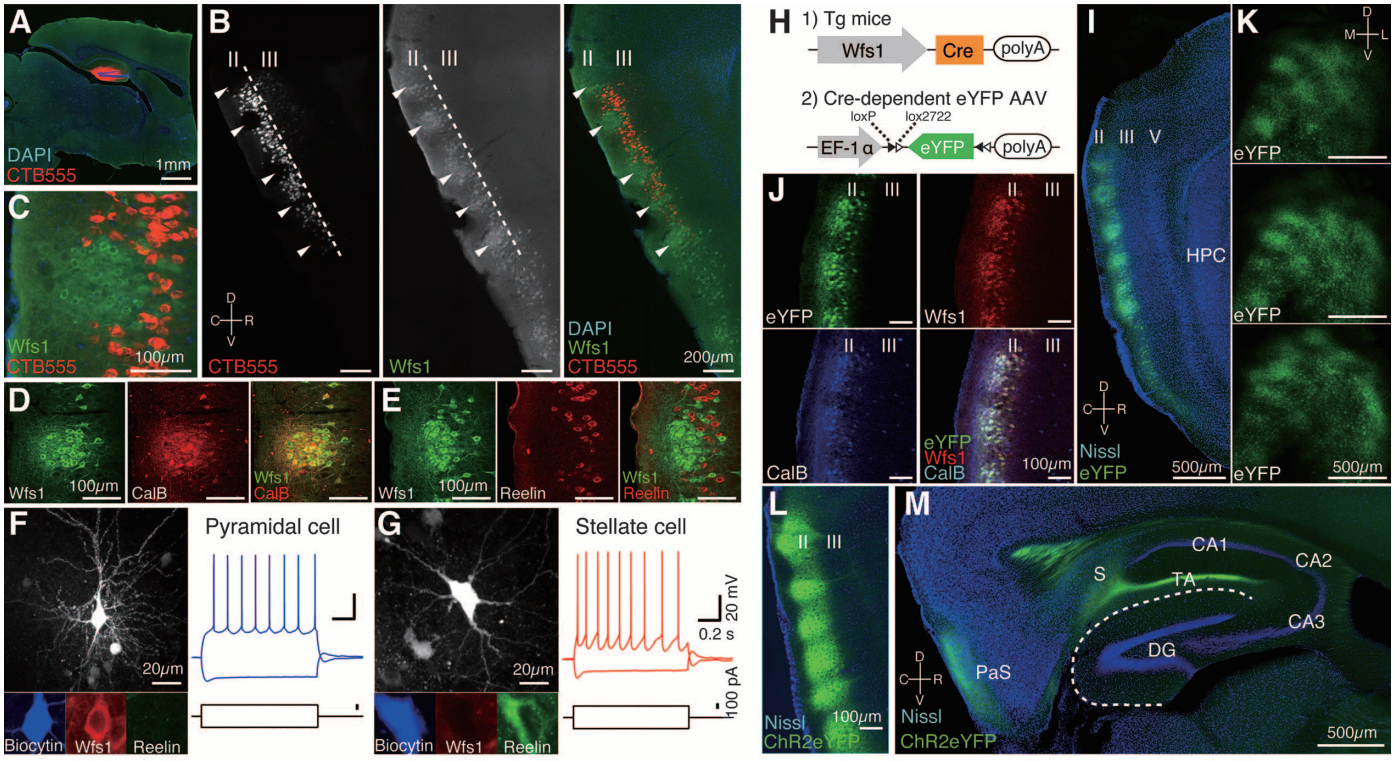


**Fig. 1. Characterizations of island cells and generation of Wfs1-Cre transgenic mice.** (**A**) Injection sites of CTB (red) in DG. (**B**) Parasagittal sections of MEC visualized with CTB-labeled cell bodies (red) and immunostained with anti-Wfs1 (green). Arrowheads indicate Wfs1-positive and CTB-negative ECIIi cells. (**C**) Magnified image from (B). (**D**) Parasagittal sections of EC immunostained with anti-Wfs1 (green) and anti–calbindin D-28K (red). (**E**) Parasagittal sections of EC immunostained with anti-Wfs1 (green) and anti-reelin (red). Wfs1-positive cells do not express reelin. (**F** and **G**) Examples of biocytin-stained Wfs1-positive pyramidal cell (F) and reelin-positive stellate cell (G) and electrophysiological responses to positive or negative current step injections. (**H**) Transgenic mouse combined with AAV injection. (**I** and **J**) Parasagittal sections of Wfs1-Cre mouse injected with $AAV_9$-EF1α-DIO-eYFP (green) and immunostained with anti-Wfs1 (red) and anti–calbindinD-28K (blue). (**K**) Tangential MEC sequential caudorostral sections of a Wfs1-Cre mouse injected with $AAV_9$-EF1α-DIO-eYFP. (**L** and **M**) Parasagittal sections of a Wfs1-Cre mouse injected with $AAV_9$-EF1α-DIO-ChR2-eYFP: injection site (EC) (L) and hippocampal innervations (M). The dotted line indicates the hippocampal fissure. TA, temporoammonic pathway; PaS, parasubiculum; S, subiculum, D, dorsal; V, ventral; R, rostral; C, caudal; L, lateral; M, medial.

by the ECIIi-INs pathway, which was demonstrated also by the in vitro study (Fig. 2O). In TFC, these mice exhibited severe freezing deficits during both training (Fig. 4E) and testing (Fig. 4F) sessions compared with the three control groups when blue-light pulses were delivered bilaterally to the CA1 areas during the entire training period. The freezing deficits were particularly large during the post-tone periods of the testing session. In contrast, the ChR2 light-on group froze as much as the control groups in response to the training context (fig. S15). When light of the same intensity and duration was delivered to the ChR2 group before (82 s before) the training period, there was no light effect on freezing (fig. S16). The delivery of blue-light pulses during the entire training period had no effect on freezing when mice were subjected to delayed fear conditioning (DFC) in which trace was omitted (Fig. 4, G and H), indicating that deficits observed in TFC (Fig. 4, E and F) are not due to an inability to encode the conditioned stimulus (CS) or unconditioned stimulus (US). A direct stimulation of SL-INs in VGAT-ChR2-eYFP transgenic mice by blue light during the training period caused freezing deficits in TFC but not in response to the context (fig. S17).

We restricted the stimulation to the trace plus foot shock period (Tr-S group) or to the tone period (To group). The light-on Tr-S group showed severe freezing deficits during both training and post-tone periods of testing sessions (Fig. 4, I and J). The patterns of freezing deficits of the light-on Tr-S group and the light-on ChR2 group were com-

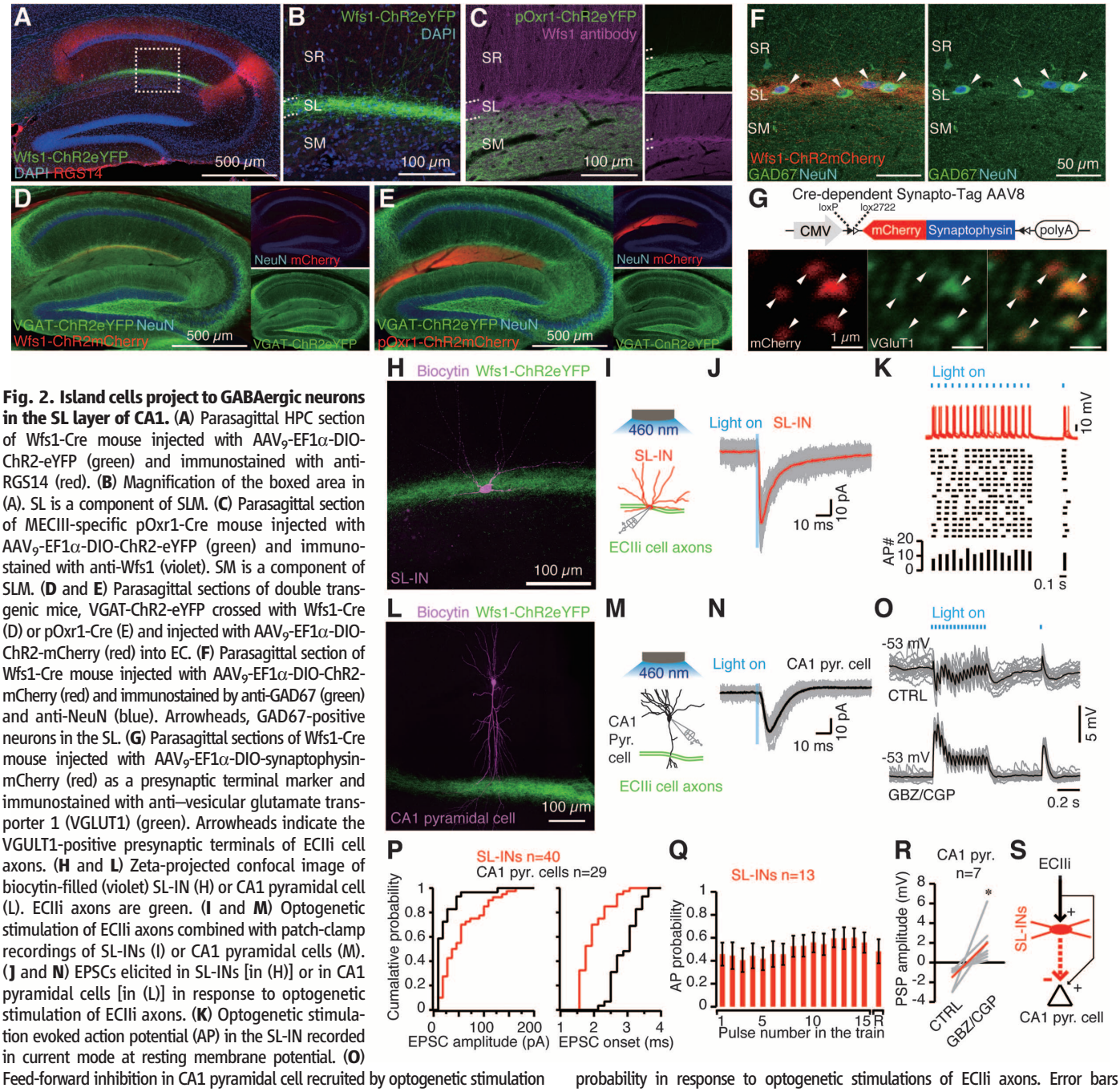


**Fig. 2. Island cells project to GABAergic neurons in the SL layer of CA1.** (**A**) Parasagittal HPC section of Wfs1-Cre mouse injected with AAV$_9$-EF1α-DIO-ChR2-eYFP (green) and immunostained with anti-RGS14 (red). (**B**) Magnification of the boxed area in (A). SL is a component of SLM. (**C**) Parasagittal section of MECIII-specific pOxr1-Cre mouse injected with AAV$_9$-EF1α-DIO-ChR2-eYFP (green) and immunostained with anti-Wfs1 (violet). SM is a component of SLM. (**D** and **E**) Parasagittal sections of double transgenic mice, VGAT-ChR2-eYFP crossed with Wfs1-Cre (D) or pOxr1-Cre (E) and injected with AAV$_9$-EF1α-DIO-ChR2-mCherry (red) into EC. (**F**) Parasagittal section of Wfs1-Cre mouse injected with AAV$_9$-EF1α-DIO-ChR2-mCherry (red) and immunostained by anti-GAD67 (green) and anti-NeuN (blue). Arrowheads, GAD67-positive neurons in the SL. (**G**) Parasagittal sections of Wfs1-Cre mouse injected with AAV$_9$-EF1α-DIO-synaptophysin-mCherry (red) as a presynaptic terminal marker and immunostained with anti–vesicular glutamate transporter 1 (VGLUT1) (green). Arrowheads indicate the VGULT1-positive presynaptic terminals of ECIIi cell axons. (**H** and **L**) Zeta-projected confocal image of biocytin-filled (violet) SL-IN (H) or CA1 pyramidal cell (L). ECIIi axons are green. (**I** and **M**) Optogenetic stimulation of ECIIi axons combined with patch-clamp recordings of SL-INs (I) or CA1 pyramidal cells (M). (**J** and **N**) EPSCs elicited in SL-INs [in (H)] or in CA1 pyramidal cells [in (L)] in response to optogenetic stimulation of ECIIi axons. (**K**) Optogenetic stimulation evoked action potential (AP) in the SL-IN recorded in current mode at resting membrane potential. (**O**) Feed-forward inhibition in CA1 pyramidal cell recruited by optogenetic stimulation of ECIIi axons. Individual traces in gray, average in black. (**P**) Kinetic of the EPSCs elicited by optogenetic stimulation of ECIIi axons. EPSCs recorded in SL-INs displayed larger amplitude [Kolmogorov-Smirnov (KS) statistic < 0.001] and faster onset (KS < 0.001) than EPSCs recorded in pyramidal cells. (**Q**) SL-INs' average AP probability in response to optogenetic stimulations of ECIIi axons. Error bars indicate SEM. (**R**) Feed-forward inhibition recruited in CA1 pyramidal cells is abolished by bath application of GABA receptor antagonists (Wilcoxon signed-rank $P < 0.05$, $n = 7$). See example in (O). (**S**) Schematic of the feed-forward inhibition. Thickness of the lines indicates connection strength.

parable during both training and testing sessions. The light-on To group did not show any significant freezing deficits during either the training or the testing session (Fig. 4, I and J).

We subjected eArch3.0eYFP-expressing (eArch group) (*17*) and eYFP only–expressing (eYFP group) Wfs1-Cre mice to in vivo recordings. The stimulation of the eArch3.0-positive ECIIi axons in the CA1 area with green light increased the multiunit activity of CA1 pyramidal cells (30% enhancement, Fig. 4B). We subjected them to TFC with green light delivered bilaterally during the entire training period. During the training session, the eArch group showed as much freezing as the control eYFP group (Fig. 4K). However, during the testing session, the eArch group displayed significantly enhanced freezing during the post-tone periods that lasted about 1 min longer compared with the control eYFP group (Fig. 4L), but freezing was unaltered in response to the context (fig. S15). Maximal levels of freezing were unaltered during training and testing sessions, although this could be due to a ceiling effect of the training protocol. Indeed, when the strength of the foot shocks was lowered, the maximal levels and the post-tone duration of freezing were greater in the eArch group compared with the control eYFP group during both training and testing sessions (Fig. 4, M and N). We injected $AAV_9$-EF1α-DIO-ChR2-mCherry into the EC of pOxr1-Cre mice. The blue-light pulse stimulation to the CA1 area increased the multiunit activity of CA1 pyramidal cells in vivo (31% enhancement, Fig. 4B). We subjected ChR2mCherry-expressing (ChR2 group) and mCherry only–expressing (mCherry group) pOxr1-Cre mice to TFC with the lower shock intensity with blue-light stimulations during the trace period. During the testing session, the ChR2 group displayed significantly enhanced freezing amplitudes and post-tone freezing duration compared with the control mCherry group (Fig. 4, O and P).

The interplay of synaptic excitation and inhibition contributes to the regulation of perception, memory, and motor behavior (*25*). A major challenge in neuroscience is to define this interplay at the levels of specific neuronal circuits and the specific cell types participating in them. We identified and characterized a neural circuit in the EC-HPC network that regulates temporal association memory, an essential component of episodic memory.

Previous studies determined that about one-third of ECII excitatory cells are made of pyramidal cells (*15*, *16*, *26*), but their projections to

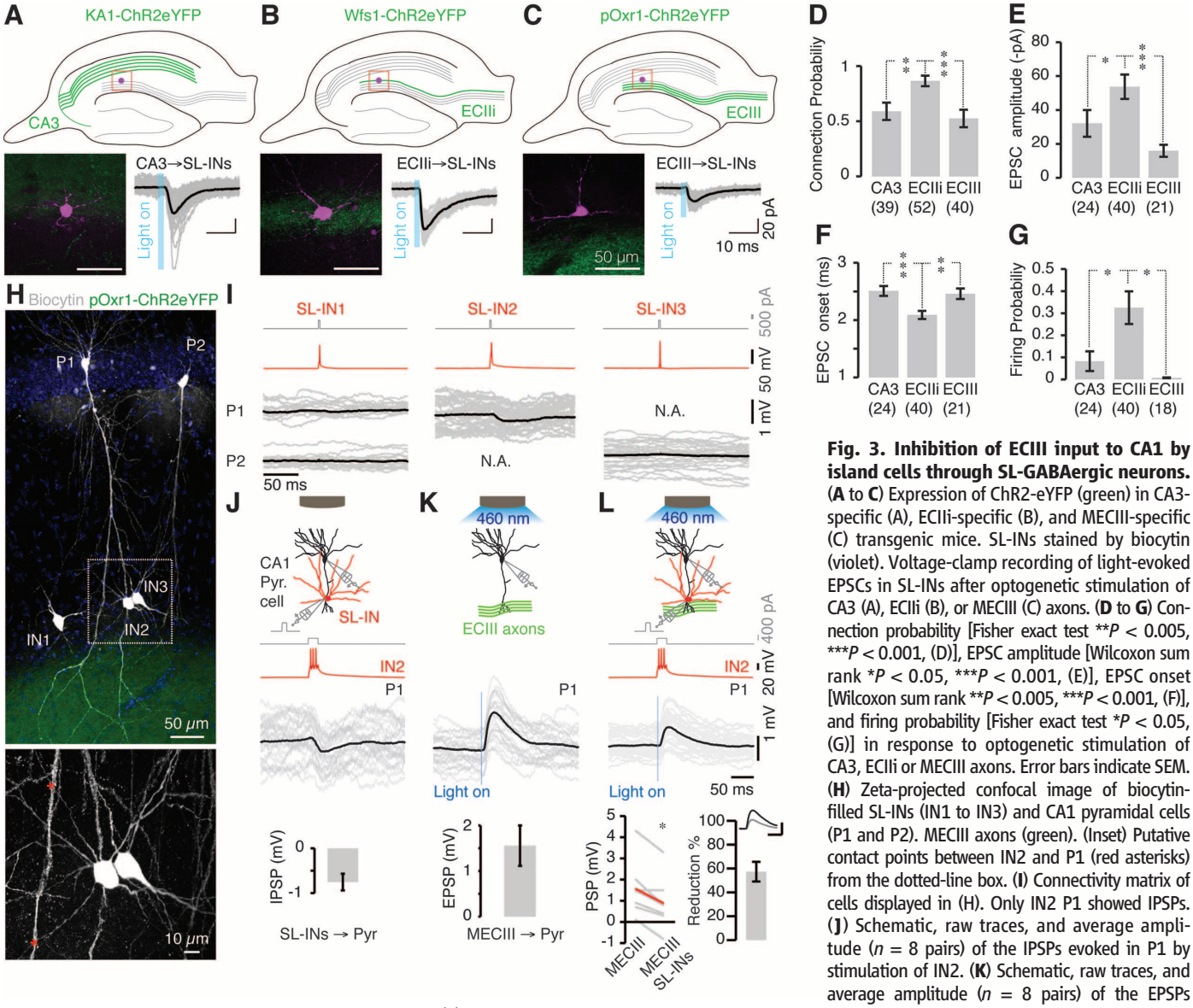


**Fig. 3. Inhibition of ECIII input to CA1 by island cells through SL-GABAergic neurons.** (**A** to **C**) Expression of ChR2-eYFP (green) in CA3-specific (A), ECIIi-specific (B), and MECIII-specific (C) transgenic mice. SL-INs stained by biocytin (violet). Voltage-clamp recording of light-evoked EPSCs in SL-INs after optogenetic stimulation of CA3 (A), ECIIi (B), or MECIII (C) axons. (**D** to **G**) Connection probability [Fisher exact test $^{**}P < 0.005$, $^{***}P < 0.001$, (D)], EPSC amplitude [Wilcoxon sum rank $^{*}P < 0.05$, $^{***}P < 0.001$, (E)], EPSC onset [Wilcoxon sum rank $^{**}P < 0.005$, $^{***}P < 0.001$, (F)], and firing probability [Fisher exact test $^{*}P < 0.05$, (G)] in response to optogenetic stimulation of CA3, ECIIi or MECIII axons. Error bars indicate SEM. (**H**) Zeta-projected confocal image of biocytin-filled SL-INs (IN1 to IN3) and CA1 pyramidal cells (P1 and P2). MECIII axons (green). (Inset) Putative contact points between IN2 and P1 (red asterisks) from the dotted-line box. (**I**) Connectivity matrix of cells displayed in (H). Only IN2 P1 showed IPSPs. (**J**) Schematic, raw traces, and average amplitude ($n$ = 8 pairs) of the IPSPs evoked in P1 by stimulation of IN2. (**K**) Schematic, raw traces, and average amplitude ($n$ = 8 pairs) of the EPSPs evoked in P1 by optogenetic stimulation of MECIII fibers. (**L**) Schematic and raw traces showing the response recorded in P1 to simultaneous stimulation of MECIII axons and IN2. Note the reduction elicited by the simultaneous stimulation when compared with optogenetic stimulation of MECIII axons only (Wilcoxon signed-rank $^{*}P < 0.05$, $n$ = 8 pairs, average in red).

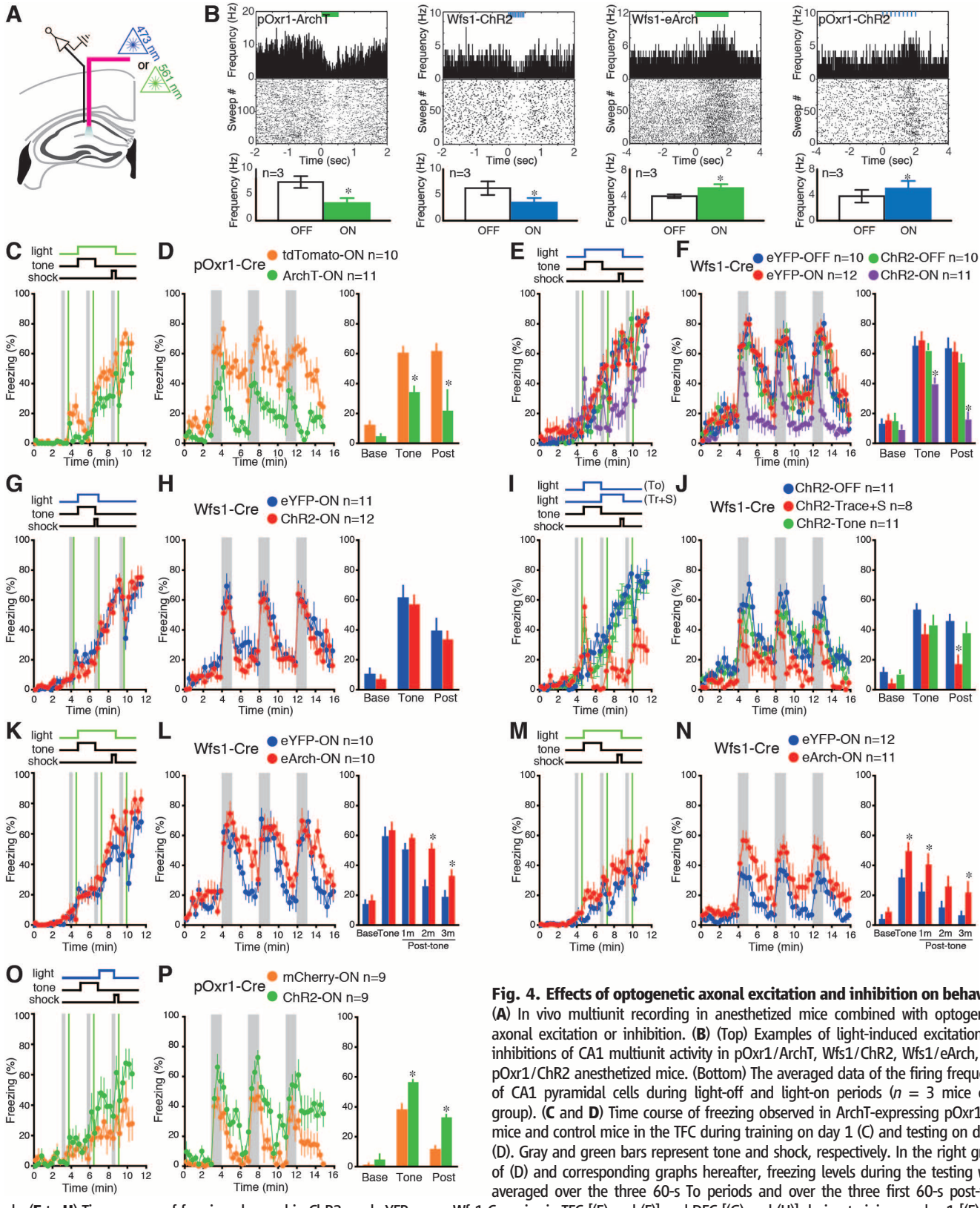


**Fig. 4. Effects of optogenetic axonal excitation and inhibition on behavior.** (**A**) In vivo multiunit recording in anesthetized mice combined with optogenetic axonal excitation or inhibition. (**B**) (Top) Examples of light-induced excitations or inhibitions of CA1 multiunit activity in pOxr1/ArchT, Wfs1/ChR2, Wfs1/eArch, and pOxr1/ChR2 anesthetized mice. (Bottom) The averaged data of the firing frequency of CA1 pyramidal cells during light-off and light-on periods ($n$ = 3 mice each group). (**C** and **D**) Time course of freezing observed in ArchT-expressing pOxr1-Cre mice and control mice in the TFC during training on day 1 (C) and testing on day 2 (D). Gray and green bars represent tone and shock, respectively. In the right graph of (D) and corresponding graphs hereafter, freezing levels during the testing were averaged over the three 60-s To periods and over the three first 60-s post-tone periods. (**E** to **H**) Time courses of freezing observed in ChR2- and eYFP-group Wfs1-Cre mice in TFC [(E) and (F)] and DFC [(G) and (H)] during training on day 1 [(E) and (G)] and testing on day 2 [(F) and (H)]. In (G), blue light was delivered during training periods (22 s). (**I** and **J**) Blue light was delivered during To (20 s) or Tr-S (22 s) periods. Time courses of freezing observed in ChR2-expressing Wfs1-Cre mice in TFC during training on day 1 (I) or testing on day 2 (J). (**K** to **N**) Time courses of freezing observed in eArch- and eYFP-group Wfs1-Cre mice in TFC [(K) and (L)] and weak TFC [(M) and (N)] during training on day 1 [(K) and (M)] and testing on day 2 [(L) and (N)]. Right graphs of (L) and (N) show freezing levels during testing on day 2 averaged over the first, second, and third 60-s post-tone periods. (**O** and **P**) Time courses of freezing observed in ChR2- and mCherry-group pOxr1-Cre mice in weak TFC during training on day 1 (O) and testing on day 2 (P). *$P < 0.05$.

SL-INs in CA1 have been unknown. The modularity of ECII neurons has been reported previously. The patchlike structures identified by anti–calbindinD-28K (*11*) and the "islets" detected by the expression of Wfs1 mRNA (*10*) probably correspond to our ECIIi cells. However, projections of these subpopulations of ECII cells into HPC have not been reported previously. Cytochrome oxidase (CO) staining revealed patches of axonal terminals in ECII that are derived from metabolically active cells (*27*, *28*). These CO-positive patches are larger than ECIIi cells and contain both calbindinD-28K–positive ECIIi cells (fig. S6) and stellate cells (*28*).

The strategic location of SL-INs, the primary target of ECIIi cells, immediately adjacent to the inner side of the SM layer where MECIII cells synapse to the distal dendrites of CA1 pyramidal cells enables ECIIi cells to suppress MECIII input by feed-forward inhibition. Our findings are consistent with previous studies pointing to the existence of a feed-forward inhibitory circuit arising from direct entorhinal inputs into CA1 (*29*, *30*). However, these earlier studies used electrical stimulation of SLM axons and hence could not distinguish ECIII and ECIIi axons that run in the SM and SL, respectively. SL-INs are connected by gap junctions (*31*). Thus, activation of ECIIi axons can evoke a depolarizing response broadly among SL-INs, which propagates through gap junctions, amplifying the effect of ECIIi cell inputs.

Our behavioral data allow for two conclusions. First, the fact that behavioral freezing in TFC was optogenetically impaired by either inhibition of MECIII input or activation of ECIIi input provides evidence for inhibition of the former input by the latter through feedforward inhibition. This conclusion is reinforced by the enhanced freezing level and the prolonged post-tone freezing period induced by eArch-mediated inactivation of the ECIIi axons. Thus, the freezing response can be regulated bidirectionally by the relative strength of MECIII and ECIIi inputs to CA1. Our data suggest that this regulatory system controls the strength of a temporal association memory as well as the duration of the expression of this memory after the recall cues cease. Such a regulation is crucial for optimal adaptive benefit; too strong an association of a particular pair of events may interfere with associations of other useful pairs, whereas too weak an association for a given pair of events will not result in an effective memory. Additionally, the ECIIi-INs pathway input can provide a specific pattern of temporal windows within which MECIII input can drive the associations.

Second, our observation that the freezing deficit was caused by the inhibition of MECIII input by the ECIIi-CA1 pathway during the Tr-S period but not during the To period indicates that the trace is not stored in CA1 and that post-tone MECIII input is crucial for the formation of temporal association memory. We propose that the source of this input could be persistent activity triggered in MECIII by the tone (*9*, *32*, *33*). Such activity will be transmitted to CA1 pyramidal cells and then to the basolateral amygdala via the EC layer V (*34*) as a CS (i.e., tone signal) coincident with the US (i.e., shock signal) to generate a fear memory engram via Hebbian synapses in the basolateral amygdala (*35*). The tone-triggered persistent activity in ECIII may also be instrumental for the prolonged post-tone freezing during recall of the temporal association memory.

Although our study has demonstrated that the feed-forward inhibition of MECIII input to CA1 pyramidal cells by the ECIIi–SL-INs pathway serves as an important mechanism for the control of temporal association memory, other circuits and/or mechanisms may also contribute to this process. For instance, a recent study described long-range projections of entorhinal interneurons into HPC interneurons, including SL-INs (*36*). This circuit could also participate in the regulation of temporal association memory by countering the effect of the ECIIi–SL-INs circuit. Another possibility is that SL-INs may contribute to the regulation of temporal association memory by rhythmic dendritic inhibition of CA1 pyramidal cells through their rhythmic activation (*22*).

CA1 pyramidal cells receive a multitude of other excitatory and inhibitory inputs (*26*) including the Schaffer collateral (SC) input from CA3 that originates from ECIIo cells. The in vitro interaction of ECIII and CA3 inputs on the activity and synaptic plasticity of CA1 pyramidal cells have been reported (*37*), but the inhibition of SC input does not seem to have a substantial effect on the TFC performance (*9*). Although the role of the direct pathway, ECIIi-CA1 pyramidal cells, has not been yet elucidated, we hypothesize that the indirect pathway from ECIIo to CA1 via the trisynaptic circuit primarily processes context and space, whereas the direct pathways from MECIII and ECIIi-SL-INs are responsible for temporal properties of episodic memory.

## References and Notes


1. E. Tulving, *Annu. Rev. Psychol.* **53**, 1–25 (2002).
2. H. Eichenbaum, *Nat. Rev. Neurosci.* **1**, 41–50 (2000).
3. E. L. Hargreaves, G. Rao, I. Lee, J. J. Knierim, *Science* **308**, 1792–1794 (2005).
4. D. Marr, *Philos. Trans. R. Soc. London Ser. B* **262**, 23–81 (1971).
5. K. Nakazawa *et al*., *Science* **297**, 211–218 (2002).
6. T. J. McHugh *et al*., *Science* **317**, 94–99 (2007).
7. G. V. Wallenstein, M. E. Hasselmo, H. Eichenbaum, *Trends Neurosci.* **21**, 317–323 (1998).
8. C. J. MacDonald, K. Q. Lepage, U. T. Eden, H. Eichenbaum, *Neuron* **71**, 737–749 (2011).
9. J. Suh, A. J. Rivest, T. Nakashiba, T. Tominaga, S. Tonegawa, *Science* **334**, 1415–1420 (2011).
10. J. Kawano *et al*., *Neurosci. Res.* **64**, 213–230 (2009).
11. Y. Fujimaru, T. Kosaka, *Neurosci. Res.* **24**, 329–343 (1996).
12. N. Tamamaki, Y. Nojyo, *Hippocampus* **3**, 471–480 (1993).
13. J. J. Couey *et al*., *Nat. Neurosci.* **16**, 318–324 (2013).
14. C. Varga, S. Y. Lee, I. Soltesz, *Nat. Neurosci.* **13**, 822–824 (2010).
15. A. Alonso, R. Klink, *J. Neurophysiol.* **70**, 128–143 (1993).
16. R. Klink, A. Alonso, *Hippocampus* **7**, 571–583 (1997).
17. J. Mattis *et al*., *Nat. Methods* **9**, 159–172 (2012).
18. S. E. Lee *et al*., *Proc. Natl. Acad. Sci. U.S.A.* **107**, 16994–16998 (2010).
19. A. Hjorth-Simonsen, J. Zimmer, *J. Comp. Neurol.* **161**, 57–70 (1975).
20. S. Zhao *et al*., *Nat. Methods* **8**, 745–752 (2011).
21. T. F. Freund, G. Buzsáki, *Hippocampus* **6**, 347–470 (1996).
22. S. Bertrand, J. C. Lacaille, *J. Physiol.* **532**, 369–384 (2001).
23. X. Han *et al*., *Front Syst Neurosci* **5**, 18 (2011).
24. O. Yizhar, L. E. Fenno, T. J. Davidson, M. Mogri, K. Deisseroth, *Neuron* **71**, 9–34 (2011).
25. J. S. Isaacson, M. Scanziani, *Neuron* **72**, 231–243 (2011).
26. P. Andersen, R. Morris, D. Amaral, T. Bliss, J. O'Keefe, *The Hippocampus Book* (Oxford Univ. Press, New York, 2007).
27. R. F. Hevner, M. T. Wong-Riley, *J. Comp. Neurol.* **326**, 451–469 (1992).
28. A. Burgalossi *et al*., *Neuron* **70**, 773–786 (2011).
29. R. M. Empson, U. Heinemann, *J. Physiol.* **484**, 707–720 (1995).
30. H. Dvorak-Carbone, E. M. Schuman, *J. Neurophysiol.* **82**, 3213–3222 (1999).
31. C. J. Price *et al*., *J. Neurosci.* **25**, 6775–6786 (2005).
32. A. V. Egorov, B. N. Hamam, E. Fransén, M. E. Hasselmo, A. A. Alonso, *Nature* **420**, 173–178 (2002).
33. T. T. Hahn, J. M. McFarland, S. Berberich, B. Sakmann, M. R. Mehta, *Nat. Neurosci.* **15**, 1531–1538 (2012).
34. O. P. Ottersen, *J. Comp. Neurol.* **205**, 30–48 (1982).
35. M. Fendt, M. S. Fanselow, *Neurosci. Biobehav. Rev.* **23**, 743–760 (1999).
36. S. Melzer *et al*., *Science* **335**, 1506–1510 (2012).
37. M. Remondes, E. M. Schuman, *Nature* **416**, 736–740 (2002).



**Acknowledgments:** We thank K. Deisseroth (ChR2 and eArch3.0 construct) and E. Boyden (ArchT construct) for providing the plasmids; R. Neve for generating the AAV-DIO-synaptophysin-mCherry; J. Martin, C. Ragion, N. Nayyar, M. Serock, L. Sultzman, M. Ragion, L. Smith, and A. Rivest for experimental help; J. Young, C. Yokoyama, T. Ryan, R. Redondo, X. Liu, and K. Mulroy for comments; and the members of Tonegawa lab for support. This work was supported by the RIKEN Brain Science Institute.


## Supplementary Materials

www.sciencemag.org/content/343/6173/896/suppl/DC1
Materials and Methods
Figs. S1 to S17
References


13 August 2013; accepted 18 December 2013
Published online 23 January 2014;
10.1126/science.1244634